Powder Technology 248 (2013) 77–83

Contents lists available at ScienceDirect

Powder Technology

journal homepage: www.elsevier.com/locate/powtec

Three-dimensional discrete element modeling of micromechanical bending tests of ceramic–polymer composite materials

M.F.H. Wolff [a,*], V. Salikov [a], S. Antonyuk [a], S. Heinrich [a], G.A. Schneider [b]

[a] Hamburg University of Technology, Institute of Solids Process Engineering and Particle Technology, Denickestr. 15, 21073 Hamburg, Germany
[b] Hamburg University of Technology, Institute of Advanced Ceramics, Denickestr. 15, 21073 Hamburg, Germany

ARTICLE INFO

Available online 20 July 2013

Keywords:
Discrete element method
Mechanical properties
Mechanical tests
Composite material
Packing density

ABSTRACT

Ceramic–polymer composite materials are used throughout materials science, but theoretical models which take into account the microstructural design to predict their mechanical properties are still not fully developed. We present an approach to use the discrete element method to model the mechanical behavior under bending load of dense composite materials made from ceramic particles which are bonded together by polymeric layers. Unlike many other modeling approaches, the internal particulate structure of the material, including the particle size distribution, packing structure, and pore structure can thus be considered. Linear-elastic bonds are created between all contacting particles to model the polymeric binder. A three-dimensional beam with a packing density of 63% is generated and its mechanical properties are tested in 3- and 4-point bending. The loading speed, loading scheme (position of the supports), and the mechanical properties of the polymeric bonds are varied and their effect on the modulus of elasticity of the material is investigated.

1. Introduction

Materials made from ceramic powders are studied and used for applications in materials sciences and industries, ranging from sophisticated machine elements to applications in everyday life, such as tableware made from porcelain. The versatile use of this material class is a consequence of a number of useful properties, including its electrical and mechanical properties, and its abundance in nature. However, the structural applications of ceramic materials are often limited by their high brittleness and scatter of mechanical properties resulting in the lack of predictability of the material failure. Furthermore, for ceramic materials it is very difficult or impossible to tailor their mechanical properties. On the other hand, polymeric materials in general exhibit a number of properties which are more or less complementary to the ones of ceramic materials, such as high ductility, adjustability, but relatively low modulus of elasticity and strength. Naturally, these two materials have been combined for many years to form composite materials.

Unlike in pure ceramics, customized mechanical properties with high strength and high fracture toughness are feasible to obtain by varying the type and amount of the two phases as well as the interface strength on different length scales [1]. To achieve a high modulus of elasticity and hardness of the composite material, it is vital to have a high amount of the ceramic phase in the material and only a small amount of the polymer. Nature has created many of its materials in exactly this way, leading to outstanding filling degrees of up to 95 vol.-% ceramic phase [2]. These materials combine high stiffness, strength, and toughness, and have been studied extensively in recent years [1,3]. Taking them as a role model for engineered materials, there is still a lot of room for improvement in the structural design of filled composite materials.

In order to develop an understanding of the complex mechanisms and structure-property relationships of composite materials, it is necessary to simulate their behavior using advanced models and modeling techniques. The influence of certain parameters under otherwise equal conditions can thus be studied much easier and more reliably than it would be the case if all structures for all parameter variations had to be synthesized and tested experimentally. In particular, it is rather straightforward to study experimentally the modulus of elasticity of polymer composites for small and medium filling degrees, but it is much harder to do the same for high packing densities (>60 vol.-%) and varying properties of the polymer under otherwise unchanged conditions, because the preparation of such samples is tedious, particularly regarding the homogeneity of the samples.

Numerous investigations have been made to study the mechanisms of mechanical reinforcement of polymers, considering the size, shape, and filling degree of the reinforcing phase [4–9]. Most of the investigations focused on relatively small (<30 vol.-%) filling degrees [10–13]. In 1963, Hill investigated the theoretical principles of elastic properties of reinforced solids [4]. Wang studied the modulus of porous materials [5]. In 1990, Ahmed and Jones reviewed the published theories and demonstrated the limitations of the existing theoretical models, which

* Corresponding author at: Institute of Solids Process Engineering and Particle Technology, Hamburg University of Technology, Hamburg, Germany. Tel.: +49 40 42878 2811; fax: +49 40 42878 2678.
E-mail address: michael.wolff@tuhh.de (M.F.H. Wolff).

0032-5910
http://dx.doi.org/10.1016/j.powtec.2013.07.009

do not yet consistently reproduce the experimental findings [6]. Very little dependence of the modulus of elasticity on the mean particle diameter was found by Spanoudakis and Young for particles of sizes from 10 to 60 μm and filling degrees between 10 and 46 vol.-% [14], and by Verbeek for particle sizes between 60 and 340 μm and a filling degree of 50 vol.-% [15]. LLorca et al. developed a roadmap for the multiscale simulation of composite materials, but focused on the simulation of fiber-reinforced composites [16].

In 2008, Fu et al. reviewed the effects of particle size and particle/matrix interface adhesion on the mechanical properties of particulate-reinforced composites with focus on small aspect ratios of the reinforcing phase [8]. They found that both strength and fracture toughness were influenced by all examined parameters, while the modulus of elasticity is significantly dependent only on the filling degree. In this paper, the micromechanical behavior of ceramic–polymer composite materials under bending is investigated using the discrete element method (DEM). With this method, it is possible to account for the discrete nature of the material on the microscale. Each ceramic particle is modeled as one discrete element, and the polymeric binder between the particles is modeled as solid bonds between these elements. Unlike most other modeling approaches, such as Finite Element Method (FEM), the particulate structure, particle size distributions and packing structure, and the pore structure are naturally considered and can be adjusted to match the desired structures.

2. Simulation method

2.1. Discrete element modeling

Since its emergence in the 1970s [17], the discrete element method (DEM) has developed into one of the primary techniques for modeling various kinds of particulate systems and processes. In the DEM, solid material is simulated as discrete and indestructive elements, which interact with each other via contact forces. The forces acting on each particle include contact forces between particles, solid bonds between particles, pressure gradients, drag, gravity, adhesive forces, etc. The forces and moments are summed up, and then they are used to numerically solve Newton's and Euler's equations of motion for individual simulation time steps. In recent years, DEM has been used to model a variety of ceramic processes and applications, including compaction of ceramic powders [18], compression tests [19,20], sintering of ceramics [21–23], modelling of fibre composites [24], and studies on two-dimensional cantilevers [25]. The DEM has been reviewed, among others, by Zhu et al. [26,27]. It has also been coupled with computational fluid dynamics to model fluidized bed processes [28–30]. However, hardly any study can be found in literature which deal with the bending or tensile testing of materials using DEM. Recently Nohut [31] studied the influence of grain size on fracture toughness of ceramics in 2D using DEM. Kempton et al. [32] investigated the compression and tensile deformation behavior of agglomerates using a sub-particle DEM õapproach, meaning that the tested agglomerates consisted of smaller particles held together by adhesive contact forces and solid bonds.

2.2. Generation of the modeled structure

The material which was modeled as the discrete particles was a ceramic material such as α-Al_2O_3, which has a density at room temperature of about 3.98 g/cm^3, a shear modulus of about 169 GPa, and a Poisson ratio of 0.23 [33]. These parameters were used as input parameters to calculate the contact force between overlapping particles. It was calculated according to the Hertz-Mindlin-Tsuji model [34–36], as summarized e. g. in [30]. Due to the linear-elastic nature of the modeled ceramic particles and the quasi-static conditions during the loading, the particle deformation is dominated by the elastic part. Thus, the coefficient of restitution was set to between 0.8 to 1 in all simulations, corresponding to a linear-elastic contact with little damping. In order to reach a high packing density without residual stresses after compaction, each particle with physical radius r_i was generated with an additional shell of thickness 6 μm, leading to a contact radius r_i^c of $r_i^c = r_i + 6$ μm. The thickness of the shell was empirically chosen, and other values can be used. However it should be clearly smaller than the particle radius, and large enough to avoid physical overlap. A contact between two particles i and j with position vectors $\vec{P_i}, \vec{P_j}$ and radii r_i, r_j was detected when the condition $\left(r_i^c + r_j^c - \left|\left(\vec{P_i} - \vec{P_j}\right)\right| \geq 0\right)$ was met (Fig. 1). For each contact the normal overlap

$$\delta_{n,ij} = r_i^c + r_j^c - \left|\left(\vec{P_i} - \vec{P_j}\right)\right| \quad (1)$$

was calculated using the contact radii r_i^c and r_j^c during the compression phase. After compression and before bond generation, the radii entering Eq. (1) were changed to the physical radii. The contact force at bond generation time $t = t_b$ was thus eliminated for almost all contacts, corresponding to a stress-free state of the specimen.

To include the contact force between contacting particles, the elastic part of the contact force was calculated according to the elastic part of the Hertz model as

$$F_n = \frac{4}{3} E^* \sqrt{r^*} \delta_n^{3/2} \quad (2)$$

using the equivalent modulus of elasticity E^* and equivalent radius r^* [30]. This force was added to the solid bond force. At $t = 0$s, the particles were generated with a size distribution shown in Fig. 2. The number of particles N was limited to 9,500 to reduce computational effort. The resulting specimens had a length on the mm-scale, which is about one order of magnitude smaller than typical sample sizes for mechanical bending tests (cm-scale). However, while the strength of brittle materials typically decreases with the sample size, no appreciable dependence of the modulus of elasticity on the sample size is to be expected for the composite structure within this size range. The particle size distribution was chosen in such a way that it models a μm-structured filler material with a mean particle diameter $d_{50,3}$ ~ 31 μm (Fig. 2). The solid volume of the sample was 0.151 mm^3. For the generation, the particles were randomly distributed in a large box ($V_{box}/V_{particles} = 132$) and then compressed by successively decreasing the box volume, until a cuboid of height $h = 256$ μm, width $w = 235$ μm and length $L = 4.27$ mm (volume $V_{specimen} = 0.257$ mm^3) was reached (Fig. 3).

The packing density ρ was determined in the following way: First a cuboid of certain size was defined within the specimen. The volume of all particles whose centres were located within this volume were summed up, and this was divided by the total volume of the chosen cuboid. This was done for several cuboid sizes and the resulting average packing density was about 63%. By doing so, the effect of the surface on the packing density could be eliminated and the true bulk density was determined.

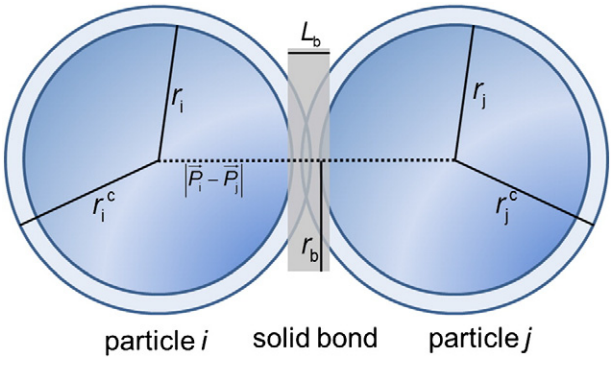

Fig. 1. Sketch of a contact with bond between two particles i and j.

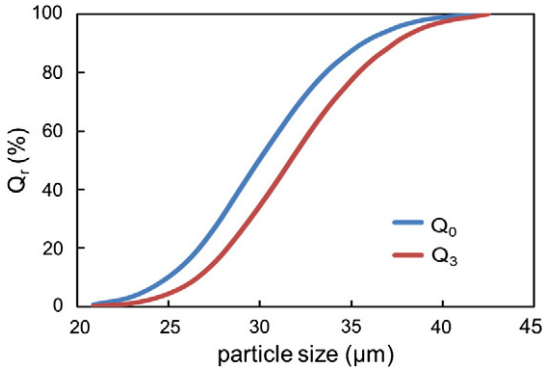

Fig. 2. Particle size distribution of the generated specimens in the DEM: Q_3 – cumulative mass-related distribution, Q_0 – cumulative number-related distribution.

At bond generation time $t = t_b$, solid bonds were generated to model the polymer forming around the ceramic particles. Bonds were generated between all contacting particles, which in total resulted in 63,281 bonds (CN = 6.7).The bonds were generated with the following input parameters: normal stiffness per unit area $\bar{k}_n$, tangential stiffness per unit area $\bar{k}_t$, and bond radius r_b. The forces and moments acting on the bonds were calculated according to linear-elastic beam theory (Euler–Bernoulli beam), as introduced into DEM by Potyondy et al. [37].

The bonding model has been used to model various kinds of materials with DEM, such as concrete [37] and agglomerate structures [38]. Polymers in general are mechanically complex materials, combining temperature dependent viscoelastic and plastic characteristics. However, for small forces and deformations the mechanical response can be well approximated by linear equations [39], justifying the approach of using linear equations to determine the elastic response of the materials for small loads. The Poisson ratio ν_b of the bond material was set to 0.42, which is a typical value for a binder polymer such as polyvinyl alcohol. Assuming cylindrical bonds, the normal stiffness per unit area is given by the modulus of elasticity divided by the bond length:

$$\bar{k}_n = \frac{E_b}{L_b}. \tag{3}$$

The Poisson ratio of the bond material then determines the ratio between normal and tangential stiffness:

$$\frac{\bar{k}_n}{\bar{k}_t} = \frac{E_b}{G_b} = 2(1+\nu). \tag{4}$$

The material parameters that were simultaneously varied during the bending tests were the normal and tangential stiffnesses, corresponding to the change of the elastic and shear moduli of the bonding polymer and/or the bond length.

3. Results and discussion

The bending behavior of the generated beam was simulated in a four-point and three-point bending setup [40,41]. Typically four-point bending tests are applied for the testing of ceramic materials, as their strength often depends on the tested sample volume. Within the two upper supports (Fig. 3), the arising stress field only depends on the height of the beam and is constant in the other two directions, and thus a larger sample volume than in three point bending can be tested under equal stress conditions.

3.1. Distribution of particles within the beam

The distribution of particle diameters and particle positions within the beam is depicted in Figs. 3 and 4. Each dot in Figs. 3 and 4 represents the centre of a particle. In Fig. 3, the diameter (y axis) of each particle is plotted as a function of beam height (Fig. 3b) and beam length (Fig. 3c). In Fig. 3b, two discrete levels are visible near each surface of the beam (maximum magnitude of z value). The two outmost levels which limit the extension of the beam in z direction are slightly inclined. This is because for the given constraint of a smooth surface, the centre of larger particles cannot be located equally far near the surface as the centre of smaller particles. By going away from the surface into the beam (smaller magnitude of z), the effect of the surface averages out, and a random packing is established. This means that while the limited height of the beam ($h/d_{particle}$ ~ 8.3) influences the distribution of particles near the surface of the beam, there is no noticeable effect anymore when going away from the surface into the inside of the material. A similar kind of

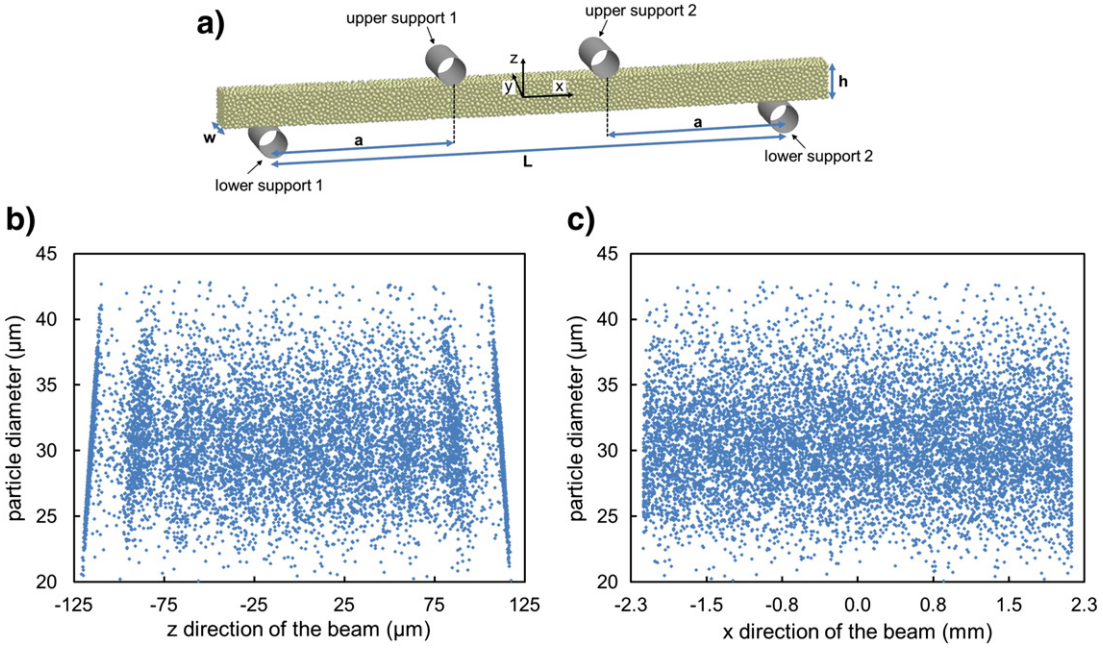

Fig. 3. Sketch of the bending setup (a). Static distribution of particle diameters along the z direction (height) (b) and the x direction (length) (c) of the beam before loading.

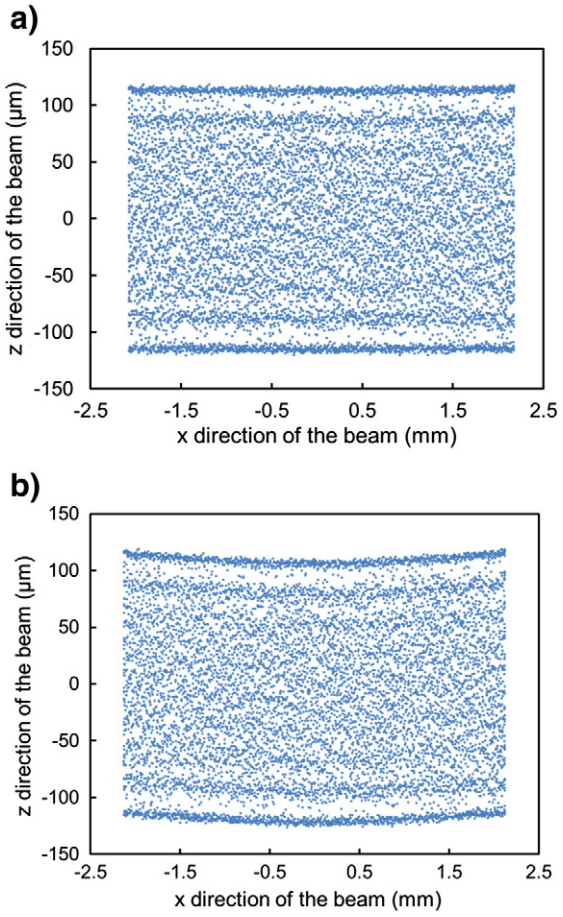

Fig. 4. Distribution of particle positions along the length (x direction) and height (z direction) of the beam before loading (a) and at a deflection $\Delta z = 4.6$ µm during loading (b).

distribution was found for the direction along the width of the beam. Due to the much larger extent of the beam in the x direction (aspect ratio > 15), no surface effect on the distribution of particle size is observed (Fig. 3c) in this direction. It can also be seen that large and small particles are statistically homogeneously distributed within the beam. Taking these aspects into consideration, a random packing of particles for the interior of the beam can be assumed. Thus for the chosen particle and specimen dimensions, there is no significant effect of the limited specimen size on the bulk packing structure and no dependence of the mechanical properties on the specimen size is to be expected.

In Fig. 4, the distribution of particle positions along the length and height of the beam are displayed before (Fig. 4a) and after (Fig. 4b) loading. Near the surface of the beam (high magnitude of z), its bending is clearly visible. In the interior of the beam, no particle movement is visible because the particles are randomly distributed.

3.2. Description of mechanical properties during elastic bending

Bending tests were carried out for several values of a. This effectively corresponds to different loading schemes, ranging from 3-point bending ($a = 0.5\ L$) to several different 4-point bending schemes. The loading scheme is an important factor in the experimental testing of materials, because some materials, especially ceramics, show different strengths under 3-point and 4-point bending. The following values of a were chosen: $a = 0.25\ L$, $a = 0.3\ L$, $a = 0.35\ L$, and $a = 0.5\ L$. For the 3-point bending test, there is only one upper support, through which all the load is applied. For the 4-point bending test, the load was applied via the two upper supports, which are moved with a constant speed (Fig. 3a). The modulus of elasticity in four-point-bending was calculated according to the Bernoulli-Euler beam theory [41] as

$$E^{4\ \mathrm{point}} = \frac{La^2\Delta F^{\mathrm{tot}}}{4I_y\Delta z}\left(1-\frac{4a}{3L}\right) \tag{5}$$

with $\Delta F^{\mathrm{tot}} = \Delta(F^{\mathrm{load}\ 1} + F^{\mathrm{load}\ 2})$ being the sum of the forces acting on each support, a is the distance between the lower and upper supports (Fig. 3a), and I_y is the second moment of area, with $I_y = \frac{1}{12}wh^3$ for a beam of width w and height h.

The parameter a can be varied from 0.25 L to 0.5 L [42], where 0.25 L is the most typically used 4-point bending setup, and $a = 0.5\ L$ is a 3-point bending test. The modulus for the 3-point bending was calculated as

$$E^{3\ \mathrm{point}} = E^{4\ \mathrm{point}}(a\rightarrow L/2) = \frac{L^3\Delta F}{48I_y\Delta z} \tag{6}$$

Before the loading, the supports were placed close to the beam without contacting any particle. They were then moved with constant speed in the z direction towards the beam until all holders were in contact with the beam. During the loading the two lower supports were fixed in space, and the upper support (3 point) or upper supports (4-point) were moved with constant speed downwards. Fig. 5 shows the loading of a beam in 3-point bending. The blue color indicates the compressive load, the red color corresponds to tensile load. In the middle of the beam, there is the neutral axis with no stress.

Several tests were carried out to validate the simulation setup. This was done by recording several force-displacement curves for different positions of the upper supports (see Fig. 6). Table 1 gives an overview over the material and simulation parameters.

For the chosen values of the normal stiffness per unit area (10^{14}, $5\cdot10^{14}$, 10^{15} N/m^3) and an assumed modulus of elasticity of the bond material of 3 GPa, a bond length was calculated according to Eq. (3), yielding $L_b = 30$ µm, $L_b = 6$ µm, and $L_b = 3$ µm respectively. For the case of $L_b = 30$ µm, the bond length is about the same as the mean particle diameter $d_{50,3}$. For the case $L_b = 3$ µm (highest stiffness), the bond length is only about 1/10 of d_p. Increasing the bond stiffness can also be thought of as an increase of the modulus of elasticity of the bond material with constant bond length, which in turn can arise from a change of polymer or from a reinforcing phase within the polymer.

During loading the beam was divided into 45 subsections to study the force network within the beam under an applied load (Fig. 6). The distribution along the width of the beam was, as expected by symmetry, rather constant throughout all tests, therefore no subdivision was done in this direction. Along the height of the specimen, the specimen was divided into three zones, representing the part of the beam which is under

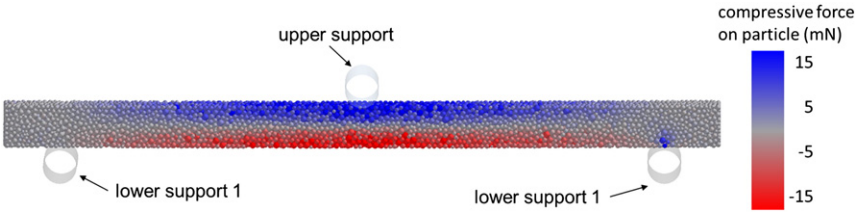

Fig. 5. Compressive force on particle during 3-point bending.

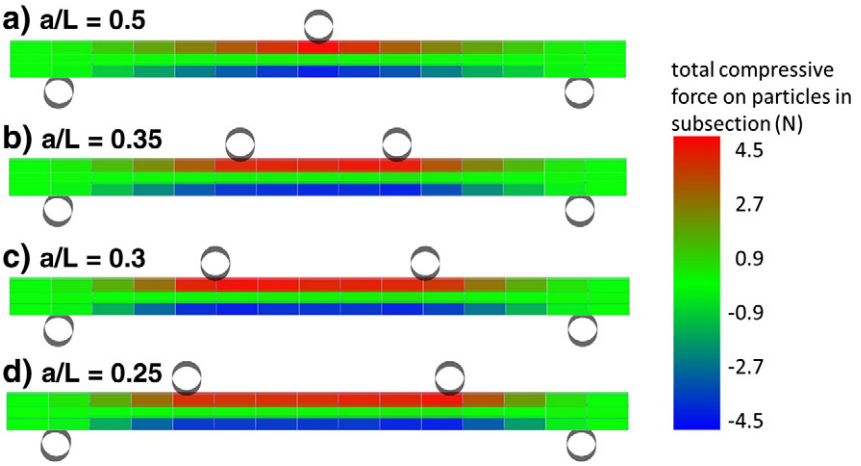

Fig. 6. Distribution of total compressive force per subsection for the different testing geometries for a bond stiffness per unit area of 10^{15} N/m^3.

compression (upper part), the neutral axis (middle part), and the part under tensile stress (lower part). In Fig. 6, the total compressive force on all particles within each subsection is depicted, where positive values mean compression, and negative values mean tension. It shows how a region of constant stress is formed (almost symmetrically for compression and tension) between the two upper supports, and how the stress is reduced towards the lower supports. It can be seen how the region of constant force (constant stress) increases for larger distance between the upper loads. The particles are not shown. The bond stiffness per unit area was chosen to be 10^{15} N/m^3 for all 4 geometries.

The used bonding model is linear-elastic, meaning that the force-displacement curve should be independent of the loading speed. This was then tested for three different speeds (1 mm/s, 5 mm/s, 10 mm/s) under otherwise identical conditions, and all three loading speeds yielded almost the same modulus of elasticity, with an increase of modulus of 1.2% from lowest to highest loading speed. The effect of a change of a/L on E was also tested (Fig. 6), and a fairly small decrease (max. 8%) of E was observed for increasing values of a/L. The fact that the force-displacement curves are independent of the loading speed can be thought of as a consequence of the lack of viscoelasticity in the bonding model with which the polymer was simulated. Therefore, even though the loading speed was rather high in order to save computational time, the bending tests represent a quasistatic testing (small loading speed) of samples in real experiments, where the viscoelastic effect is not pronounced. Table 2 lists the calculated modulus of elasticity of the beam for the varied parameters. For the varied loading speed, the normal stiffness per unit area was set to the medium value ($5 \cdot 10^{14}$ N/m^3), and for the varied loading schemes, it was set to the highest value (10^{15} N/m^3).

Fig. 7 shows the force-displacement curves which were obtained by varying the normal stiffness per unit area $\overline{k}_n$. The ratio a/L was set to 0.5 and $v_{load} = 10$ mm/s for these tests. For small displacements, a settling of the beam can be seen. After the settling, a linear increase of force with displacement of the upper load can be observed. As can be seen, the corresponding modulus of elasticity, which is proportional to the slope of the curce, increases with increasing normal stiffness per unit area.

Table 1
Simulation parameters.

Variable	Symbol	Unit	Value
Distance between lower and upper support	a	mm	0.9 , 1.08 , 1.26 , 1.8
Coordination number	CN	–	6.7
Median particle diameter	$d_{50,3}$	μm	31
Shear modulus of particles and supports	G_{cer}	GPa	169
Height of the beam	h	μm	256
Normal bond stiffness per unit volume	$\overline{k}_n$	N/m^3	10^{14}, $5 \cdot 10^{14}$, 10^{15}
Ratio of normal and tangential stiffnesses	$\overline{k}_n/\overline{k}_t$	–	1.16
Length of the beam	L_{beam}	mm	4.27
Distance between lower supports	L	mm	3.6
Number of particles	N	–	9500
Radius of the supports	r_{load}	μm	100
Bond radius	r_b	μm	11
Simulation time step	t_{sim}	s	$3 \cdot 10^{-10}$
Loading speed	v_{load}	mm/s	1 , 5 , 10
Width of the beam	w	μm	235
Packing density	ρ	vol.-%	63
Poisson ratio of particles and supports	ν_{cer}	–	0.23

Table 2
Modulus of elasticity versus the varied parameters loading speed v_{load}, positioning of the supports a/L, and normal stiffness of the solid bond $\overline{k}_n$.

v_{load} (mm/s)	E (GPa)	a / L	E (GPa)	$\overline{k}_n$ (N/m^3)	E (GPa)
1	16.8	0.25	35.9	$1 \cdot 10^{14}$	3.7
5	16.9	0.3	34.1	$5 \cdot 10^{14}$	17.2
10	17.2	0.35	33.1	$1 \cdot 10^{15}$	33.2
		0.5	33.2		

4. Summary and conclusions

The discrete element method was used for the first time to model the mechanical behavior of beams in 3- and 4-point bending consisting of > 60 vol.-% ceramic particles bonded together by polymer bonds. The approach was tested and validated under various conditions (varied loading speed, positioning of the supports, and bond stiffnesses). The formation of a region of constant stress was observed for the 4 point bending setups. The modulus of elasticity was found to vary almost

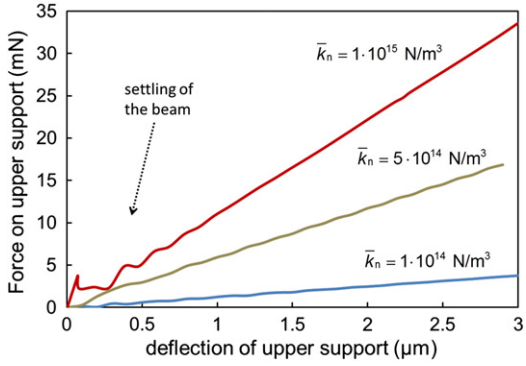

Fig. 7. Force on the upper support for the three-point bending setup as a function of the displacement of the upper support.

linearly with the bond stiffness, while no dependence of the modulus of elasticity on the positioning of the supports or on the loading speed was observed. As a linear-elastic bonding model without viscoelasticity was used, which corresponds to quasistatic loading, this is in good agreement with the theoretical expectations and verifies the validity of this simulation approach for micromechanical bending tests of beams made from particulate matter. By using the DEM, certain aspects of the presented material system, which all influence the mechanical behavior, such as its packing structure, particle size distributions, the distribution of pores, sliding, and changes in the orientation of particles during loading can be considered. This will turn it into a powerful modeling tool also within the area of material research. Future investigations will focus on studying the material failure mechanisms of such composite beams by allowing plastic deformations and introducing equivalent stresses and failure criteria for the bonds.

Nomenclature

a	distance between upper and lower support
CN	coordination number
E	modulus of elasticity
E^*	equivalent modulus of elasticity
d_{particle}	particle diameter
F_{n}	normal force
G	shear modulus
G_{cer}	shear modulus of particles and supports
h	height of the beam
I_{y}	second moment of area
$\overline{k}_{\text{n}}$	normal bond stiffness per unit area
$\overline{k}_{\text{t}}$	tangential bond stiffness per unit area
L	distance between lower supports
L_{b}	bond length
L_{beam}	length of the beam
N	number of particles
$\overrightarrow{P_{\text{i}}},\overrightarrow{P_{\text{j}}}$	position vector of particle i, j
r_{b}	bond radius
r_{load}	radius of the load cylinders
$r_{\text{i}},r_{\text{j}}$	radius of particles i, j
$r_{\text{i}}^{\text{c}},r_{\text{j}}^{\text{c}}$	contact radius of particles i, j
r^*	equivalent radius
ρ	packing density
t	simulation time
t_{b}	bond generation time
t_{sim}	simulation time step
V	volume
v	loading speed
ν	Poisson ratio
w	width of the specimen
ΔF	increase of normal force on a support during a considered time interval
Δz	distance the upper support or supports move downwards during a considered time interval
δ_{n}	normal overlap between two particles

Acknowledgements

We gratefully acknowledge financial support from the German Research Foundation (DFG) via SFB 986 "M^3", project A3 and A6, and from the Cluster of Excellence "Integrated Materials Systems" within the Landesexzellenzinitiative Hamburg, Germany.

References

[1] H. Gao, Application of fracture mechanics concepts to hierarchical biomechanics of bone and bone-like materials, International Journal of Fracture 138 (2006) 101–137.
[2] A.P. Jackson, J.F. Vincent, R.M. Turner, The mechanical design of nacre, Proceedings of the Royal Society of London, Series B: Biological Sciences 234 (1988) 415–440.
[3] P. Fratzl, R. Weinkamer, Nature's hierarchical materials, Progress in Materials Science 52 (2007) 1263–1334.
[4] R. Hill, Elastic properties of reinforced solids - some theoretical principles, Journal of the Mechanics and Physics of Solids 11 (1963) 357–372.
[5] J.C. Wang, Young's modulus of porous materials Part1: Theoretical derivation of modulus-porosity correlation, Journal of Materials Science 19 (1984) 801–808.
[6] S. Ahmed, F.R. Jones, A review of particulate reinforcement theories for polymer composites, Journal of Materials Science 25 (1990) 4933–4942.
[7] Z.K. Zhu, Y. Yang, J. Yin, Z.N. Qi, Preparation and properties of organosoluble polyimide/silica hybrid materials by sol-gel process, Journal of Applied Polymer Science 73 (1999) 2977–2984.
[8] S.-Y. Fu, X.-Q. Feng, B. Lauke, Y.-W. Mai, Effects of particle size, particle/matrix interface adhesion and particle loading on mechanical properties of particulate-polymer composites, Composites Part B: Engineering 39 (2008) 933–961.
[9] K. Brandt, V. Salikov, H. Oezcoban, P. Staron, A. Schreyer, L.A.S.A. Prado, K. Schulte, S. Heinrich, G.A. Schneider, Novel ceramic–polymer composites synthesized by compaction of polymer-encapsulated TiO(2)-nanoparticles, Composites Science and Technology 72 (2011) 65–71.
[10] M.E. Dekkers, D. Heikens, The effect of interfacial adhesion on the tensile behavior of polystyrene glass-bead composites, Journal of Applied Polymer Science 28 (1983) 3809–3815.
[11] D.M. Bigg, Mechanical-properties of particulate filled polymers, Polymer Composites 8 (1987) 115–122.
[12] Y.C. Ou, F. Yang, Z.Z. Yu, New conception on the toughness of nylon 6/silica nanocomposite prepared via in situ polymerization, Journal of Polymer Science Part B: Polymer Physics 36 (1998) 789–795.
[13] E. Reynaud, T. Jouen, C. Gauthier, G. Vigier, J. Varlet, Nanofillers in polymeric matrix: a study on silica reinforced PA6, Polymer 42 (2001) 8759–8768.
[14] J. Spanoudakis, R.J. Young, Crack-propagation in a glass particle-filled epoxy-resin 1. Effect of particle-volume fraction and size, Journal of Materials Science 19 (1984) 473–486.
[15] C.J. Verbeek, The influence of interfacial adhesion, particle size and size distribution on the predicted mechanical properties of particulate thermoplastic composites, Materials Letters 57 (2003) 1919–1924.
[16] J. LLorca, C. Gonzalez, J.M. Molina-Aldareguia, J. Segurado, R. Seltzer, F. Sket, M. Rodriguez, S. Sadaba, R. Munoz, L.P. Canal, Multiscale Modeling of Composite Materials: a Roadmap Towards Virtual Testing, Advanced Materials 23 (2011) 5130–5147.
[17] P.A. Cundall, O.D. Strack, Discrete numerical-model for granular assemblies, Geotechnique 29 (1979) 47–65.
[18] P. Pizette, C.L. Martin, G. Delette, P. Sornay, F. Sans, Compaction of aggregated ceramic powders: From contact laws to fracture and yield surfaces, Powder Technology 198 (2010) 240–250.
[19] C. Thornton, M.T. Ciomocos, M.J. Adams, Numerical simulation of diametrical compression tests on agglomerates, Powder Technology 140 (2004) 258–267.
[20] S. Antonyuk, S. Heinrich, J. Tomas, N.G. Deen, M.S. van Buijtenen, J.A.M. Kuipers, Energy absorption during compression and impact of dry elastic-plastic spherical granules, Granular Matter 12 (2010) 15–47.
[21] D. Jauffres, C.L. Martin, A. Lichtner, R.K. Bordia, Simulation of the elastic properties of porous ceramics with realistic microstructure, Modelling and Simulation in Materials Science and Engineering 20 (2012).
[22] G. Jefferson, G.K. Haritos, R.M. McMeeking, The elastic response of a cohesive aggregate – a discrete element model with coupled particle interaction, Journal of the Mechanics and Physics of Solids 50 (2002) 2539–2575.
[23] A. Wonisch, T. Kraft, M. Moseler, H. Riedel, Effect of Different Particle Size Distributions on Solid-State Sintering: A Microscopic Simulation Approach, Journal of the American Ceramic Society 92 (2009) 1428–1434.
[24] H. Fujita, G. Jefferson, R.M. McMeeking, F.W. Zok, Mullite/alumina mixtures for use as porous matrices in oxide fiber composites, Journal of the American Ceramic Society 87 (2004) 261–267.
[25] F.A. Tavarez, M.E. Plesha, Discrete element method for modelling solid and particulate materials, International Journal for Numerical Methods in Engineering 70 (2007) 379–404.
[26] H.P. Zhu, Z.Y. Zhou, R.Y. Yang, A.B. Yu, Discrete particle simulation of particulate systems: Theoretical developments, Chemical Engineering Science 62 (2007) 3378–3396.
[27] H.P. Zhu, Z.Y. Zhou, R.Y. Yang, A.B. Yu, Discrete particle simulation of particulate systems: A review of major applications and findings, Chemical Engineering Science 63 (2008) 5728–5770.
[28] B.H. Xu, A.B. Yu, Numerical simulation of the gas-solid flow in a fluidized bed by combining discrete particle method with computational fluid dynamics, Chemical Engineering Science 52 (1997) 2785–2809.
[29] N.G. Deen, M.S. van Annaland, M.A. van der Hoef, J.A.M. Kuipers, Review of discrete particle modeling of fluidized beds, Chemical Engineering Science 62 (2007) 28–44.
[30] L. Fries, S. Antonyuk, S. Heinrich, S. Palzer, DEM-CFD modeling of a fluidized bed spray granulator, Chemical Engineering Science 66 (2011) 2340–2355.
[31] S. Nohut, Prediction of crack-tip toughness of alumina for given residual stresses with parallel-bonded-particle model, Computational Materials Science 50 (2011) 1509–1519.
[32] L. Kempton, D. Pinson, S. Chew, P. Zulli, A. Yu, Simulation of macroscopic deformation using a sub-particle DEM approach, Powder Technology 223 (2012) 19–26.
[33] R.G. Munro, Evaluated material properties for a sintered alpha-alumina, Journal of the American Ceramic Society 80 (1997) 1919–1928.
[34] H. Hertz, Über die Berührung fester elastischer Körper, Journal für die reine und angewandte Mathematik 92 (1882) 156–171.
[35] R.D. Mindlin, H. Deresiewicz, Elastic spheres in contact under varying oblique forces, Journal of Applied Mechanics, Transactions ASME 20 (1953) 327–344.

[36] Y. Tsuji, T. Tanaka, T. Ishida, Lagrangian numerical simulation of plug flow of cohesionless particles in a horizontal pipe, Powder Technology 71 (1992) 239–250.
[37] D.O. Potyondy, P.A. Cundall, A bonded-particle model for rock, International Journal of Rock Mechanics 41 (2004) 1329–1364.
[38] S. Antonyuk, S. Palis, S. Heinrich, Breakage behaviour of agglomerates and crystals by static loading and impact, Powder Technology 206 (2011) 88–98.
[39] G.R. Strobl, The Physics of Polymers: Concepts for Understanding Their Structures and Behavior, Springer, Berlin Heidelberg New York, 2007.
[40] S. Timoshenko, The Strength of Materials: Part I: Elementary Theory and Problems, Robert E. Krieger Publishing Co., Inc., New York, 1955.
[41] M.G. Gere, Mechanics of Materials, 6th ed. Bill Stenquist, Belmont, CA, USA, 2004.
[42] H. Czichos, T. Saito, L. Smith, Handbook of Materials Measurement Methods, Springer, Heidelberg, 2006.